

# Plain $s$ -wave superconductivity near magnetic criticality: Enhancement of attractive electron-boson coupling vertex corrections

Rina Tazai<sup>1</sup>, Youichi Yamakawa<sup>1</sup>, Masahisa Tsuchiizu<sup>2</sup>, and Hiroshi Kontani<sup>1</sup>

<sup>1</sup> *Department of Physics, Nagoya University, Furo-cho, Nagoya 464-8602, Japan.*

<sup>2</sup> *Department of Physics, Nara Women's University, Nara 630-8506, Japan*

(Dated: October 11, 2018)

Recent experiments revealed that the plain  $s$ -wave state without any sign-reversal emerges in various metals near magnetic criticality. To understand this counter-intuitive phenomenon, we study the gap equation for the multiorbital Hubbard-Holstein model, by analyzing the vertex correction (VC) due to the higher-order electron-correlation effects. We find that the phonon-mediated orbital fluctuations are magnified by the VC for the susceptibility ( $\chi$ -VC). In addition, the charge-channel attractive interaction is enlarged by the VC for the coupling-constant ( $U$ -VC), which is significant when the interaction has prominent  $\mathbf{q}$ -dependences; therefore the Migdal theorem fails. Due to both  $\chi$ -VC and  $U$ -VC, the plain  $s$ -wave state is caused by the small electron-phonon interaction near the magnetic criticality against the repulsive Coulomb interaction. We find that the direct Coulomb repulsion for the plain  $s$ -wave Cooper pair is strongly reduced by the “multiorbital screening effect.”

Keywords: orbital fluctuations, self-consistent vertex correction theory, magnetic quantum criticality

It is widely believed that the spin-fluctuations are harmful for the conventional  $s$ -wave superconductivity. However, recent experiments have revealed that the plain  $s$ -wave state without any sign-reversal emerges in some strongly-correlated metals near the magnetic instability. For example, plain  $s$ -wave superconductivity with high  $T_c$  is reported in heavily electron-doped FeSe families ( $T_c = 60 \sim 100\text{K}$ ) [1, 2] and in  $\text{A}_3\text{C}_{60}$  ( $\text{A} = \text{K, Rb, Cs}$ ;  $T_c > 30\text{K}$ ) [3]. In both compounds, electron-phonon ( $e$ -ph) interaction may play a crucial role in the pairing mechanism, as discussed in Refs. [4–10]. Even so, a fundamental question is why the high- $T_c$  plain  $s$ -wave state appears against the repulsive interaction by spin-fluctuations. More surprisingly, the plain  $s$ -wave state is reported in heavy-fermion superconductor  $\text{CeCu}_2\text{Si}_2$  near the magnetic phase, according to the measurements of the specific heat, penetration depth, thermal conductivity, and electron irradiation effect on  $T_c$  [11, 12].

Therefore, it is a significant problem for theorists to establish a general mechanism of the plain  $s$ -wave superconductivity in strongly correlated electron systems. One important feature of these  $s$ -wave superconductors would be the orbital degrees of freedom. In this case, in principle, the pairing glue for the plain  $s$ -wave state may be realized by the orbital fluctuations. The two possible origins of the orbital fluctuations are the higher-order many-body process given by the vertex correction (VC) [13] and the  $e$ -ph interaction [14]. The significant questions are (i) whether these two different origins of the orbital fluctuations (*i.e.*, the VC due to Coulomb interaction and the  $e$ -ph interaction) cooperate or not, (ii) why the high- $T_c$  plain  $s$ -wave state is realized against the strong magnetic fluctuations, and (iii) how the plain  $s$ -wave Cooper pairs escape from the strong direct Coulomb repulsion in multiorbital systems.

In this paper, we analyze a canonical two-orbital model in detail in order to resolve the above-mentioned funda-

mental questions (i)-(iii). We study the pairing mechanism in the presence of strong magnetic fluctuations and small phonon-mediated attractive interaction, by considering the VC for the orbital susceptibility ( $\chi$ -VC) and the VC for the pairing interaction ( $U$ -VC) consistently. In both VCs, the significant contributions come from the Aslamazov-Larkin (AL) processes, which represent the strong orbital-spin interference driven by the electron correlation [13]. Due to both VCs, weak  $e$ -ph interaction is enough to realize the high- $T_c$  plain  $s$ -wave state near the magnetic quantum criticality. The present theory explains the characteristic phase diagram in typical strongly-correlated plain  $s$ -wave superconductors such as FeSe,  $\text{A}_3\text{C}_{60}$ , and  $\text{CeCu}_2\text{Si}_2$ . We also find that the direct Coulomb repulsion for the intra-orbital  $s$ -wave Cooper pair is reduced by the “multiorbital screening effect.”

We start from the two-orbital Hubbard-Holstein model on the square lattice  $H = H_0 + H_U + H_{\text{ph}}$ , where  $H_0 = \sum_{\mathbf{k}, \sigma} \sum_{l, m} \xi_{\mathbf{k}}^{l, m} c_{\mathbf{k}l\sigma}^\dagger c_{\mathbf{k}m\sigma}$  is the kinetic term, and  $H_U = \frac{1}{4} \sum_i \sum_{ll'mm'} \sum_{\sigma\sigma'\rho\rho'} U_{l, l'; m, m'}^{0; \sigma\sigma' \rho\rho'} c_{i l \sigma}^\dagger c_{i l' \sigma'} c_{i m \rho} c_{i m' \rho'}^\dagger$  is the on-site Coulomb interaction term. Here,  $i$  is a lattice site index,  $c_{\mathbf{k}l\sigma}^\dagger$  ( $c_{\mathbf{k}l\sigma}$ ) is the creation (annihilation) operator of  $d$ -electrons with wave-vector  $\mathbf{k}$ , orbital  $l$ , and spin  $\sigma$ .  $l = 1$  (2) represents the orbital  $d_{xz}$  ( $d_{yz}$ ).  $\xi_{\mathbf{k}}^{l, m}$  is defined as  $\xi_{\mathbf{k}}^{1, 1} = -2t \cos k_x - 2t'' \cos k_y$ ,  $\xi_{\mathbf{k}}^{2, 2} = -2t \cos k_y - 2t'' \cos k_x$ , and  $\xi_{\mathbf{k}}^{1, 2} = \xi_{\mathbf{k}}^{2, 1} = -4t' \sin k_x \sin k_y$ . Hereafter, we set the hopping parameters as  $(t, t', t'') = (1, 0.1, 0.1)$ . The unit of energy in the present study is  $t = 1$ , and the electron filling is fixed as  $n_e = 2.30$ . The two Fermi surfaces (FSs), FS  $\alpha$  and FS  $\beta$ , are shown in Fig. 1(a), where  $\theta$  is the angle of the  $\mathbf{k}$  on each FS. The bare multiorbital Coulomb interaction  $U_{l, l'; m, m'}^{0; \sigma\sigma' \rho\rho'}$  is composed of the intra-orbital Coulomb interaction  $U$ , inter-orbital one  $U'$ , Hund's coupling  $J$ , and pair hopping  $J'$  [15].  $U_{l, l'; m, m'}^{0; \sigma\sigma' \rho\rho'}$  is uniquely decomposed into the spin-channel and charge-channel;  $\hat{U}^{0; \sigma\sigma' \rho\rho'} = \frac{1}{2} \hat{U}^{0; s} \vec{\sigma}_{\sigma\sigma'} \cdot \vec{\sigma}_{\rho\rho'} + \frac{1}{2} \hat{U}^{0; c} \delta_{\sigma, \sigma'} \delta_{\rho', \rho}$ ,

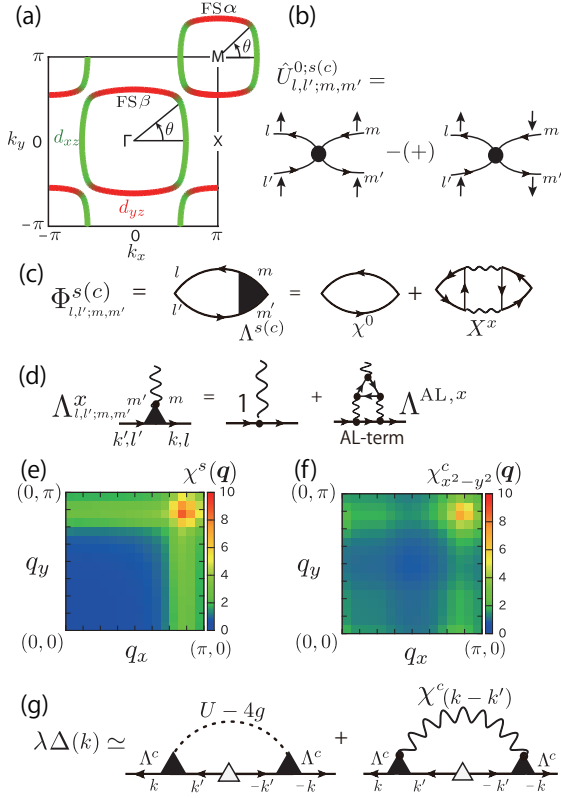


FIG. 1: (Color online) (a) FSs of the two-orbital model composed of  $d_{xz}$  (green) and  $d_{yz}$  (red) orbitals. The nesting between FS  $\alpha$  and FS  $\beta$  causes the spin and orbital fluctuations at  $\mathbf{Q} \simeq (0.8\pi, 0.8\pi)$ . (b) Multi-orbital Coulomb interaction for the spin- (charge-) channel. (c) Irreducible susceptibility with the  $\chi$ -VC. (d) Dressed electron-boson coupling due to the AL process. (e)  $\mathbf{q}$ -dependences of the (e) total spin susceptibility  $\chi^s(\mathbf{q})$  and (f) orbital susceptibility  $\chi_{x^2-y^2}^c(\mathbf{q})$  at  $(\alpha_S, \alpha_C) = (0.92, 0.93)$ . (g) Linearized gap equation with the three-point VC ( $U$ -VC).

where  $\vec{\sigma}$  is the Pauli matrix vector and  $\hat{U}^{0;s(c)}$  is the spin- (charge-) channel Coulomb interaction shown in Fig. 1(b). Their expressions are given in the Supplementary Material (SM):A [16]. Hereafter, we simply put  $J = J' = (U - U')/2$ .

In addition,  $H_{\text{ph}}$  is the phonon-related term given by  $H_{\text{ph}} = \omega_D \sum_i b_i^\dagger b_i + \eta \sum_i (b_i^\dagger + b_i)(\hat{n}_i^{xz} - \hat{n}_i^{yz})$ , where  $\hat{n}_i^l$  is an electron number operator for orbital  $l$ ,  $b_i^\dagger$  ( $b_i$ ) is a phonon creation (annihilation) operator,  $\eta$  is the coupling constant between electrons and  $B_{1g}$ -symmetry phonon, and  $\omega_D$  is the phonon frequency. The phonon-mediated retarded interaction is  $-g(\omega_j) \sum_i (\hat{n}_i^{xz} - \hat{n}_i^{yz})(\hat{n}_i^{xz} - \hat{n}_i^{yz})$  [14], where  $g(\omega_j) = g \frac{\omega_D^2}{\omega_D^2 + \omega_j^2}$  and  $g = \frac{2\eta^2}{\omega_D} (> 0)$ .  $\omega_j = 2j\pi T$  is the boson Matsubara frequency with integer  $j$ . In the present model,  $B_{1g}$  orbital fluctuations are induced by the  $\chi$ -VC even for  $g = 0$ . Due to the  $\chi$ -VC, the  $B_{1g}$  orbital fluctuations are strongly enhanced by introducing the small  $g$  given by the  $B_{1g}$  phonon. Such enhancement

is not realized by non  $B_{1g}$  phonons.

Now, we derive the spin and charge susceptibilities by analyzing the  $\chi$ -VC for the charge-channel self-consistently, based on the self-consistent vertex correction (SC-VC) method [13]. Hereafter, we fix the parameters  $J/U = 0.08$  and  $T = 5 \times 10^{-2}$ , and use the notations  $k = (\mathbf{k}, \epsilon_n) = (\mathbf{k}, (2n+1)\pi T)$  and  $q = (\mathbf{q}, \omega_j) = (\mathbf{q}, 2j\pi T)$ . We adopt  $N_k = 32 \times 32$   $\mathbf{k}$ -meshes and 256 Matsubara frequencies. In the present model, the spin ( $x = s$ ) and charge ( $x = c$ ) susceptibilities are

$$\hat{\chi}^x(q) = \hat{\Phi}^x(q)[\hat{1} - \hat{C}^x \hat{\Phi}^x(q)]^{-1}, \quad (1)$$

where  $\hat{\chi}^x$ ,  $\hat{\Phi}^x$ , and  $\hat{C}^x$  are  $2^2 \times 2^2$  matrices in the orbital basis, and  $\hat{\Phi}^x(q) = \hat{\chi}^0(q) + \hat{X}^x(q)$  is the irreducible susceptibility. We explain the matrix expressions of  $\hat{\chi}^x(q)$  and  $\hat{X}^x(q)$  in the SM:B and SM:C, respectively [16].  $\hat{X}^x(q)$  is the  $\chi$ -VC given by the AL process. Its diagrammatic expression is shown in Fig. 1(c), which contains the three-point VC,  $\hat{\Lambda}^x(k, k')$ , as shown in Fig. 1(d). The solid and wavy lines represent the electron Green function  $\hat{G}(k)$  and  $\hat{\chi}^x(q)$ , respectively. The bare susceptibility is given by  $\chi_{l,l',m,m'}^0(q) = -\frac{T}{N_k} \sum_k G_{l,m}(k+q)G_{m',l'}(k)$ , where  $G_{l,m}(k)$  is the Green function in the orbital basis without the self-energy. The spin (charge) Stoner factor  $\alpha_{S(C)}$  is given by the largest eigenvalue of  $\hat{C}^{s(c)}\hat{\Phi}^{s(c)}(q)$ . Here, we calculate  $\hat{X}^c(q)$  self-consistently, by neglecting  $\hat{X}^s(q)$  since it is less important [17]. In the random phase approximation (RPA), both  $\hat{X}^s$  and  $\hat{X}^c$  are dropped.

As we explain in the SM:B [16], the interaction terms are  $\hat{C}^s \equiv \hat{U}^{0;s}$  and  $\hat{C}^c \equiv \hat{U}^{0;c} - \hat{g}(\omega_j)$ , where  $\hat{g}$  is the phonon-mediated interaction given as  $g_{l,l',m,m'}(\omega_j) \equiv -2g(\omega_j) \cdot \delta_{l,l'}\delta_{m,m'}(2\delta_{l,m} - 1)$ . Here, we neglect the ladder-diagram for the phonon-mediated interaction by assuming the relation  $\omega_D \ll W_{\text{band}}$  (bandwidth). In this case,  $\alpha_S$  is independent of  $g$  if we put  $\hat{X}^s = 0$  [14]. Note that the orbital-fluctuations are caused by the cooperation between  $\chi$ -VC and  $g$ , even when  $\omega_D \gg W_{\text{band}}$ .

Figures 1(e) and 1(f) show the obtained total spin susceptibility,  $\chi^s(\mathbf{q}) = \sum_{l,m} \chi_{l,l',m,m'}^s(\mathbf{q})$ , and orbital susceptibility with respect to the  $B_{1g}$  orbital operator  $\hat{n}_{xz} - \hat{n}_{yz}$ ,  $\chi_{x^2-y^2}^c(\mathbf{q}) = \sum_{l,m} (-1)^{l+m} \chi_{l,l',m,m'}^c(\mathbf{q})$ , respectively. The used parameters are  $(U, g) = (2.1, 0.15)$ , and the realized Stoner factors are  $(\alpha_S, \alpha_C) = (0.92, 0.93)$ . The spin susceptibility is enlarged due to the nesting between FS  $\alpha$  and FS  $\beta$ , and the strong orbital susceptibility is induced by the  $\chi$ -VC and the small  $g$  is due to the  $B_{1g}$  phonon. The antiferro-orbital ordered phase is realized when  $\alpha_C \geq 1$ . More detailed results are shown in the SM:B [16].

Next, we analyze the linearized gap equation beyond the Migdal-Eliashberg scheme given as [18]

$$\lambda\Delta^a(\theta, \epsilon_n) = -\frac{\pi T}{(2\pi)^2} \sum_{a', \epsilon_m} \int_0^{2\pi} \frac{d\theta'}{v_{a', \theta'}} \left| \frac{\partial \mathbf{k}_{a', \theta'}}{\partial \theta'} \right|$$

$$\times \frac{\Delta^{a'}(\theta', \epsilon_m)}{|\epsilon_m|} V^{a,a'}(\theta, \epsilon_n, \theta', \epsilon_m), \quad (2)$$

which is diagrammatically expressed in Fig. 1(g).  $\Delta^a(\theta, \epsilon_n)$  and  $\lambda$  are the singlet superconducting gap function on the FS  $a$  ( $a = \alpha, \beta$ ) and its eigenvalue, respectively.  $V^{a,a'}(\theta, \epsilon_n, \theta', \epsilon_m)$  is the pairing interaction in the band basis.  $\mathbf{k}_{a,\theta}$  and  $v_{a,\theta}$  are the Fermi momentum and the Fermi velocity on FS  $a$ , respectively.

Using  $\hat{\chi}^{s(c)}(q)$  derived from the SC-VC method, the pairing interaction in the orbital basis is given as [18]

$$\hat{V}(k, k') = \frac{3}{2} \hat{I}^{\Lambda,s}(k, k') - \frac{1}{2} \hat{I}^{\Lambda,c}(k, k') - \hat{C}^s, \quad (3)$$

which is transformed to  $V^{a,a'}(\theta, \epsilon_n, \theta', \epsilon_m)$  by using the unitary matrix  $u_{l,a}(\mathbf{k}) = \langle l, \mathbf{k} | a, \mathbf{k} \rangle$ . Here,  $\hat{I}^{\Lambda,x}(k, k') = \hat{\Lambda}^x(k, k') \hat{I}^x(k - k') \hat{\Lambda}^x(-k, -k')$ , and  $\hat{I}^x(k - k') = \hat{C}^x \hat{\chi}^x(k - k') \hat{C}^x + \hat{C}^x$ .  $\hat{\Lambda}^x(k, k')$  is the three-point vertex with the AL-type  $U$ -VC shown in Fig. 1(d), and  $\bar{\Lambda}_{l,l';m,m'}^x(k, k') \equiv \Lambda_{m',m;l,l}^x(k, k')$  [18]. Then, the effective Coulomb interaction dressed by the  $U$ -VC is  $\hat{U}^x(k, k') = \hat{\Lambda}^x(k, k') \hat{C}^x$ , which is given in the SM:C [16]. Since the contribution to the  $U$ -VC from  $\chi^s(q)$  dominates over the one from  $\chi^c(q)$  even for  $\alpha_S \sim \alpha_C$ , as explained in Refs. [17, 18], we can safely set  $g = 0$  in for calculating  $\hat{\Lambda}^x$ .

Here, we explain the important role of the  $U$ -VC on the superconductivity. In Figs. 2(a) and 2(b), we show the charge- and spin-channel enhancement factors in the band basis at  $\epsilon_n = \epsilon_{n'} = \pi T$  defined as

$$\left| \Lambda_{a,a'}^{s(c)}(\theta, \theta') \right|^2 \equiv \left| \sum_{l,l',m} \Lambda_{l,l';m,m}^{s(c)}(k, k') u_{l,a}^*(\theta) u_{l',a'}(\theta') \right|^2. \quad (4)$$

Here, we set  $U = 2.1$  ( $\alpha_S = 0.92$ ). Figure 2(a) means that  $|\Lambda^c|^2 \gg 1$ , when both Fermi points ( $\theta$  and  $\theta'$ ) are composed of the same orbital. In contrast, Fig. 2(b) means that  $|\Lambda^s|^2 \ll 1$ , for the same orbital. Their  $\alpha_S$ -dependences are shown in Fig. 2(c), which are very similar to Fig. 8(a) for  $n_e = 2.67$  in Ref. [19]. The obtained relation  $|\Lambda^c|^2 \gg 1$  for  $\alpha_S \lesssim 1$  originates from the AL-type  $U$ -VC for the charge-channel  $\Lambda^{\text{AL},c}(q) \propto \sum_p \chi^s(p) \chi^s(p+q)$ , which is explained in Fig. 2(d) and in Ref. [18]. This relation owing to the AL-processes has been confirmed by the functional-renormalization-group (fRG) analysis in Refs. [19]. In the fRG method, the higher-order VCs, even higher order than Figs. 1(c) and (d), are generated in a systematic and unbiased way.

Hereafter, we solve the gap equation (2) numerically and simply set  $g(\omega_j) = g$  by neglecting the retardation effect. This approximation leads to the underestimation of the plain  $s$ -wave state. In addition, we neglect both the  $U$ -VC and  $\chi$ -VC for finite  $\omega_j$ , and also drop the crossing pairing interaction introduced in Ref. [18]. These simplifications also lead to the underestimation of the plain  $s$ -wave state [18]. We summarize the approximations used in the numerical study in the SM:C [16].

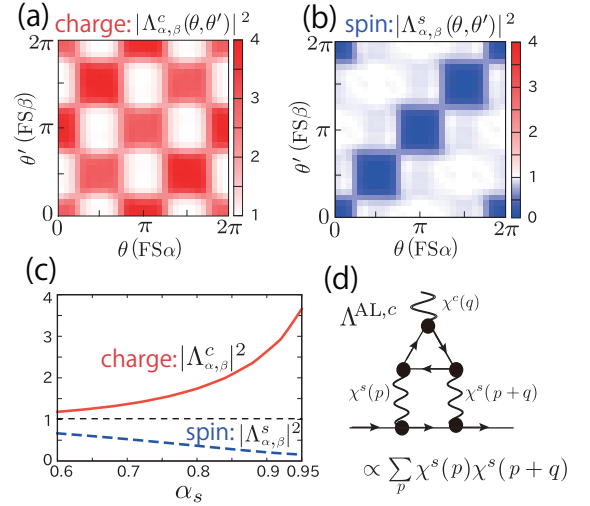


FIG. 2: (Color online) (a)  $|\Lambda_{\alpha,\beta}^c(\theta, \theta')|^2$  and (b)  $|\Lambda_{\alpha,\beta}^s(\theta, \theta')|^2$  for the lowest frequency.  $\theta$  ( $\theta'$ ) represents the Fermi point on the FS  $\alpha$  ( $\beta$ ). (c)  $\alpha_S$  dependence of  $|\Lambda_{\alpha,\beta}^{s(c)}(\theta, \theta')|^2$  at  $\theta = \theta' = 0$ . (d) AL-type  $U$ -VC for the charge channel.

In Fig. 3(a), we show the largest eigenvalue with the phase boundary between three  $s$ -wave states given in Figs. 3(b)-3(d), which we call the phase diagram below. In the nodal  $s_{++}$  ( $s_{+-}$ ) state,  $\Delta^\alpha(N\pi/2, \epsilon_n)$  and  $\Delta^\beta(N\pi/2, \epsilon_n)$  have the same (opposite) sign for  $N = 0, 1, 2, 3$ . In Fig. 3(a) and Fig. S3(a) in the SM:D [16], the full-gap  $s_{++}$  state without any sign reversal corresponds to the largest eigenvalue for a wide region with  $\alpha_C \geq 0.8$ . The obtained  $\lambda$  for the full-gap  $s_{++}$  state is very large, since the attractive (repulsive) interaction is enlarged (suppressed) by  $|\Lambda^{c(s)}|^2$  [18–20]. Thus,  $T_c$  for the full-gap  $s$ -wave state is expected to be high. In contrast,  $\lambda$  for nodal  $s_{++}$  and  $s_{+-}$  states is very small.

Figure 3(e) shows the  $\alpha_S$ -dependence of  $\lambda$  at  $\alpha_C = 0.93$ . When the  $U$ -VC is included,  $\lambda$  for the full-gap  $s_{++}$  state drastically increases with  $\alpha_S$ . In contrast, the full-gap  $s_{++}$  state disappears in the phase diagram if the  $U$ -VC is neglected (=Migdal approximation [21]), as shown in Fig. 3(f). Although the pairing interaction has the small energy scale, the Migdal theorem fails due to its strong  $\mathbf{q}$ -dependence. Therefore, the significance of the  $U$ -VC for the plain  $s$ -wave state is clearly confirmed.

We see in Fig. 3(a) that, the strong orbital fluctuations  $\alpha_C \lesssim 1$  are realized just  $g \approx 0.15$  ( $\lesssim U/10$ ) for  $\alpha_S \gtrsim 0.9$ . By following Ref. [22], orbital susceptibility for  $\alpha_C \lesssim 1$  is approximately given as  $\chi_{x^2-y^2}^c(\mathbf{Q}) \sim \Phi^c(\mathbf{Q}) [1 - (2U' - U + 4g)\Phi^c(\mathbf{Q})]^{-1}$ , where  $\Phi^c(\mathbf{Q})$  is the intra-orbital irreducible susceptibility. Due to the existence of  $U'$ ,  $\alpha_C = (2U' - U + 4g)\Phi^c(\mathbf{Q})$  reaches unity by introducing the small  $g$  due to the  $B_{1g}$  phonon. In addition, the required  $g$  for  $\alpha_C = 1$  is reduced if the relation  $\Phi^c(\mathbf{Q}) \gg \chi^0(\mathbf{Q})$  is realized by the AL-VC. Therefore, the strong orbital fluctuations are induced by the coop-

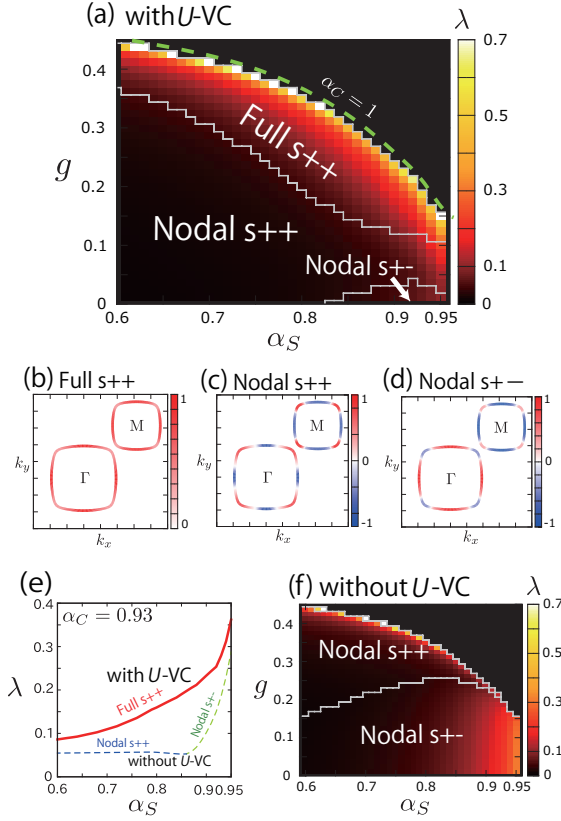


FIG. 3: (Color online) (a) Obtained phase diagram for the  $s$ -wave states in the presence of the  $U$ -VC. The gap functions for the (b) full-gap  $s_{++}$  state at  $g = 0.2$ , (c) nodal  $s_{++}$  state at  $g = 0.06$ , and (d) nodal  $s_{+-}$  state at  $g = 0.04$ , for  $\alpha_S = 0.92$ . The antiferro-orbital order occurs when  $\alpha_C \geq 1$ . (e)  $\alpha_S$  dependence of  $\lambda$  at  $\alpha_C = 0.93$ . The eigenstate is full-gap  $s_{++}$  state with  $U$ -VC, whereas it is nodal  $s_{++(+)}$  state without  $U$ -VC. (f) Phase diagram obtained by neglecting the  $U$ -VC.

eration between the  $B_{1g}$  phonon ( $g$ ) and the  $\chi$ -VC.

To summarize, the full-gap  $s_{++}$  wave state is stabilized by the charge-channel pairing interaction  $V^c \simeq \frac{1}{2}\{U - 4g + (2U' - U + 4g)^2 \chi_{x^2-y^2}^c(\mathbf{Q})\} |\Lambda^c|^2$ , which takes large negative value when  $\alpha_C \lesssim 1$  and  $|\Lambda^c|^2 \gg 1$ . The latter condition is realized when  $\alpha_S \lesssim 1$  due to the AL-VC. We verified in the SM:E [16] that the full-gap  $s_{++}$  state corresponds to the largest eigenvalue for a wide filling range if the  $U$ -VC is included in the gap equation. Note that the momentum dependence of the  $\Lambda^x(k, k')$  is quite important since the full-gap  $s_{++}$  phase disappears if we apply the local approximation to  $U$ -VC;  $\Lambda_{\text{loc}}^x(\epsilon_n, \epsilon_{n'}) \equiv \langle \Lambda^x(k, k') \rangle_{\mathbf{k}, \mathbf{k}' \in \text{FS}}$ , as shown in the SM:D [16]. In the SM:F and SM:G, we discuss that the full-gap  $s_{++}$  wave state is further stabilized by introducing the dilute impurities and by considering the retardation effect, respectively.

Finally, we explain that the direct Coulomb repulsion for the  $s$ -wave Cooper pair is strongly reduced by the ‘‘multiorbital screening effect.’’ Figures 4(a) and 4(b)

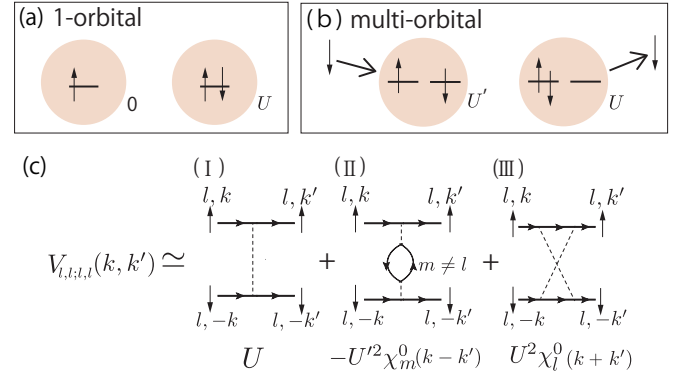


FIG. 4: (Color online) Schematic depairing processes for the intra-orbital Cooper pair caused by the direct Coulomb interaction, in (a) one-orbital and (b) two-orbital cases. In (b), the energy cost for the intra-orbital pair is reduced to  $\sim (U - U')$  due to the ‘‘multiorbital screening effect.’’ (c) Pairing interaction for the intra-orbital Cooper pair up to second-order. The process (II) exists only in multiorbital models. Here,  $\chi_l^0 \equiv \chi_{l,t,l}^0$ .

show the schematic depairing processes for the ‘‘intra-orbital Cooper pair’’ for the single- and multi-orbital models, respectively. Here, the effect of  $J$  is neglected for simplicity. The energy cost for the intra-orbital Cooper pair, which is  $\sim U$  in the single-orbital model, is drastically reduced to  $\sim (U - U')$  in the multi-orbital model. This reduction is caused by the screening due to the electrons on other orbitals. Thus, we call this effect the multiorbital screening. Figure 4(c) shows the pairing interaction for the intra-orbital Cooper pair up to second-order. We assume  $G_{l,m} = G_l \cdot \delta_{l,m}$  for simplicity. The process (II), which exists only in the multiorbital models, reduces the direct Coulomb depairing given by (I). This multiorbital screening effect is prominent when  $U' \chi_{m,m;m,m}^0 \sim O(1)$  for  $m \neq l$ . Note that the depairing is suppressed further by the retardation effect.

We comment on other theoretical studies. Based on the dynamical-mean-field-theory (DMFT) or variational cluster approach (VCA), mechanisms of the plain  $s$ -wave state due to the electron correlation (together with the  $e$ -ph interaction) have been discussed in Refs. [8–10, 23, 24]. In  $\text{CeCu}_2\text{Si}_2$ , both the valence fluctuation and orbital fluctuation scenarios have been discussed in Refs. [25, 26].

In summary, we proposed the mechanism of the plain  $s$ -wave state in strongly correlated metals with the weak  $B_{1g}$   $e$ -ph interaction. We demonstrated that the strong orbital fluctuations emerge due to the cooperation between the  $\chi$ -VC and the  $B_{1g}$   $e$ -ph interaction, and the orbital-fluctuation-mediated attractive force is enhanced by the charge-channel  $U$ -VC. In contrast, the repulsive force due to the spin fluctuations is reduced by the spin-channel  $U$ -VC. In addition, the direct Coulomb repulsion for the intra-orbital cooper pair is strongly reduced by the

multiorbital screening effect. The plain  $s$ -wave state has a large eigenvalue in the vicinity of the magnetic quantum criticality as shown in Fig. 3(e). The present theory may explain the strongly-correlated plain  $s$ -wave superconductivity in FeSe,  $A_3C_{60}$ , and  $CeCu_2Si_2$ .

We stress that the charge-channel  $U$ -VC is enhanced by the AL-VC even in one-orbital models, which explains the result of the quantum Monte Carlo study for the two-dimensional one-orbital Hubbard model in Ref. [27].

We are grateful to Y. Matsuda, T. Shibauchi, S. Kasahara, and S. Onari for their useful comments and discussions. This study has been supported by Grants-in-Aid for Scientific Research from MEXT of Japan.

- 
- [1] C. H. P. Wen, H. C. Xu, C. Chen, Z. C. Huang, X. Lou, Y. J. Pu, Q. Song, B. P. Xie, Mahmoud Abdel-Hafiez, D. A. Chareev, A. N. Vasiliev, R. Peng, and D. L. Feng, *Nat. Commun.* **7**, 10840 (2016).
- [2] Y. J. Yan, W. H. Zhang, M. Q. Ren, X. Liu, X. F. Lu, N. Z. Wang, X. H. Niu, Q. Fan, J. Miao, R. Tao, B. P. Xie, X. H. Chen, T. Zhang, and D. L. Feng, *Phys. Rev. B* **94**, 134502 (2016).
- [3] Y. Takabayashi and L. Prassides, *Phil. Trans. R. Soc. A* **374**, 20150320 (2016).
- [4] S. Rebec, T. Jia, C. Zhang, M. Hashimoto, D. Lu, R. Moore, and Z. Shen, *Phys. Rev. Lett.* **118**, 067002 (2017).
- [5] Y. Zhou and A. J. Millis, *Phys. Rev. B* **93**, 224506 (2016).
- [6] S. Choi, W.-J. Jang, H.-J. Lee, J. M. Ok, H. W. Choi, A. T. Lee, A. Akbari, K. Nakatsukasa, Y. K. Semertzidis, Y. Bang, S. Johnston, J. S. Kim, and J. Lee, arXiv:1608.00886.
- [7] L. Rademaker, Y. Wang, T. Berlijn, and S. Johnston, *New J. Phys.* **18**, 022001 (2016).
- [8] M. Capone, M. Fabrizio, and E. Tosatti, *Phys. Rev. Lett.* **86**, 5361 (2001).
- [9] Y. Nomura, S. Sakai, M. Capone, and R. Arita, *Science Advances* **1**, e1500568 (2015).
- [10] M. Kim, Y. Nomura, M. Ferrero, P. Seth, O. Parcollet, and A. Georges, *Phys. Rev. B* **94**, 155152 (2016).
- [11] T. Yamashita, T. Takenaka, Y. Tokiwa, J. A. Wilcox, Y. Mizukami, D. Terazawa, Y. Kasahara, S. Kittaka, T. Sakakibara, M. Konczykowski, S. Seiro, H. S. Jeevan, C. Geibel, C. Putzke, T. Onishi, H. Ikeda, A. Carrington, T. Shibauchi, and Y. Matsuda, arXiv:1703.02800.
- [12] S. Kittaka, Y. Aoki, Y. Shimura, T. Sakakibara, S. Seiro, C. Geibel, F. Steglich, Y. Tsutsumi, H. Ikeda, and K. Machida, *Phys. Rev. B* **94**, 054514 (2016).
- [13] S. Onari and H. Kontani, *Phys. Rev. Lett.* **109**, 137001 (2012).
- [14] H. Kontani and S. Onari, *Phys. Rev. Lett.* **104**, 157001 (2010).
- [15] T. Takimoto, *Phys. Rev. B* **62**, R14641(R) (2000).
- [16] Supplementary Material
- [17] Y. Yamakawa, S. Onari, and H. Kontani, *Phys. Rev. X* **6**, 021032 (2016).
- [18] Y. Yamakawa and H. Kontani, arXiv:1611.05375.
- [19] R. Tazai, Y. Yamakawa, T. Tsuchiizu, and H. Kontani, *Phys. Rev. B* **94**, 115155 (2016).
- [20] S. Onari, Y. Yamakawa, and H. Kontani, *Phys. Rev. Lett.* **112**, 187001 (2014).
- [21] A. B. Migdal, *J. Exptl. Thoret. Phys.* **34**, 1438 (1958).
- [22] Y. Ohno, M. Tsuchiizu, S. Onari, and H. Kontani, *J. Phys. Soc. Jpn.* **82**, 013707 (2012).
- [23] O. Bodensiek, R. Zitko, M. Vojta, M. Jarrell, and T. Pruschke, *Phys. Rev. Lett.* **110**, 146406 (2013).
- [24] K. Masuda and D. Yamamoto, *Phys. Rev. B* **91**, 104508 (2015).
- [25] K. Miyake and S. Watanabe, arXiv:1704.00114.
- [26] K. Hattori, *J. Phys. Soc. Jpn.* **79**, 114717 (2010).
- [27] Z. B. Huang, W. Hanke, E. Arrighoni, and D. J. Scalapino, *Phys. Rev. B* **68**, 220507(R) (2003).

[Supplementary Material]

Plain  $s$ -wave superconductivity near the magnetic criticality: Enhancement of attractive electron-boson coupling vertex corrections

Rina Tazai, Youichi Yamakawa, Masahisa Tsuchiizu, and Hiroshi Kontani

**A: Multiorbital Coulomb interaction**

In the main text, we studied the two-orbital Hubbard-Holstein model. Hereafter, we use the variables  $a \sim h, l, l', m, m'$  as orbital indices in this Supplementary Material (SM). First, we explain the multiorbital Coulomb interaction, which is uniquely decomposed into the spin-channel and charge-channel parts as [1]

$$U_{l,l';m,m'}^{0;\sigma\sigma'\rho\rho'} = \frac{1}{2}U_{l,l';m,m'}^{0;s}\vec{\sigma}_{\sigma\sigma'} \cdot \vec{\sigma}_{\rho'\rho} + \frac{1}{2}U_{l,l';m,m'}^{0;c}\delta_{\sigma,\sigma'}\delta_{\rho',\rho}. \quad (\text{S1})$$

Here, the matrix elements of the spin- and charge-channel Coulomb interactions are

$$U_{l,l';m,m'}^{0;s} = \begin{cases} U & (l = l' = m = m') \\ U' & (l = m \neq l' = m') \\ J & (l = l' \neq m = m') \\ J' & (l = m' \neq l' = m) \\ 0 & (\text{otherwise}) \end{cases}, \quad (\text{S2})$$

$$U_{l,l';m,m'}^{0;c} = \begin{cases} -U & (l = l' = m = m') \\ U' - 2J & (l = m \neq l' = m') \\ -2U' + J & (l = l' \neq m = m') \\ -J' & (l = m' \neq l' = m) \\ 0 & (\text{otherwise}) \end{cases}. \quad (\text{S3})$$

**B: Multiorbital spin and charge susceptibilities**

In the main text, we use the  $2^2 \times 2^2$  matrix representation for the multiorbital spin (charge) susceptibility  $\hat{\chi}^x(q)$  ( $x = s, c$ ). The matrix elements of  $\hat{\chi}^x(q)$  in Eq. (1) in the main text is given as  $\chi_{l,l';m,m'}^x(q) = \sum_{a,b} \Phi_{l,l';a,b}^x(q) [\hat{1} - \hat{C}^x \hat{\Phi}^x(q)]_{a,b;m,m'}^{-1}$ .

Here, we explain the orbital dependence of the spin (charge) susceptibility for  $(U, g) = (2.1, 0.15)$ . The Stoner factors are  $(\alpha_S, \alpha_C) = (0.92, 0.93)$ . We show  $\chi_{1,1;1,1}^{s(c)}(\mathbf{q})$  and  $\chi_{1,1;2,2}^{s(c)}(\mathbf{q})$  in Figs. S1(a)-S1(d) since  $\chi_{l,l';m,m'}^{s(c)}(\mathbf{q})$  has large value only for  $l = l'$  and  $m = m'$  in the present model. We stress that  $\chi_{x_2-y_2}^c(\mathbf{q})$  with respect to the orbital polarization  $\Delta \hat{n} \equiv \hat{n}_{xz} - \hat{n}_{yz}$  is enlarged due to large negative value of  $\chi_{1,1;2,2}^c(\mathbf{q})$  at  $\mathbf{q} \approx (0.8\pi, 0.8\pi)$  shown in Fig. S1(d). In contrast, the total charge susceptibility for the charge operator  $\hat{n}_{\text{tot}} \equiv \hat{n}_{xz} + \hat{n}_{yz}$ , which is given as  $\chi_{\text{tot}}^c(\mathbf{q}) = \sum_{l,m} \chi_{l,l;m,m}^c(\mathbf{q})$ , is not enhanced by the  $\chi$ -VC at all.

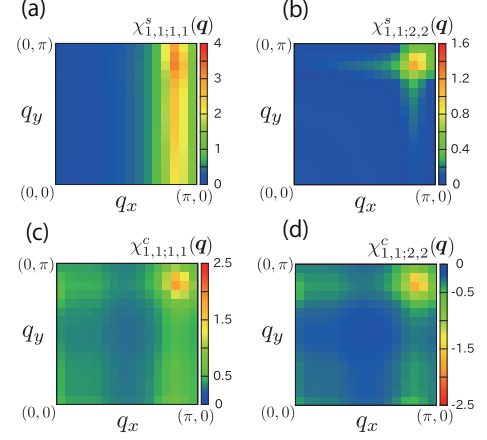


FIG. S1: (Color online) The  $\mathbf{q}$ -dependence of the obtained susceptibilities of (a)  $\chi_{1,1;1,1}^s(\mathbf{q})$ , (b)  $\chi_{1,1;2,2}^s(\mathbf{q})$ , (c)  $\chi_{1,1;1,1}^c(\mathbf{q})$ , and (d)  $\chi_{1,1;2,2}^c(\mathbf{q})$ .

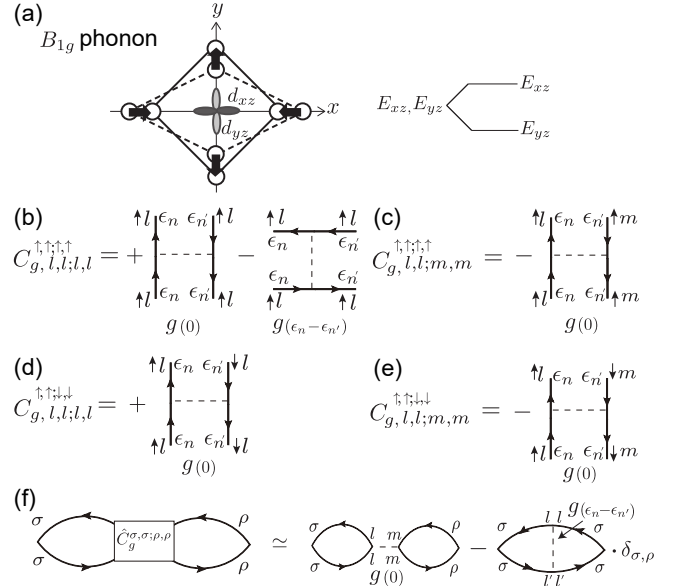


FIG. S2: (Color online) (a) The electron-phonon coupling caused by  $B_{1g}$ -symmetry distortion. The diagrammatic expressions for (b)  $C_{g,l,l;l,l}^{\uparrow,\uparrow;\uparrow,\uparrow}$ , (c)  $C_{g,l,l;m,m}^{\uparrow,\uparrow;\uparrow,\uparrow}$ , (d)  $C_{g,l,l;l,l}^{\uparrow,\uparrow;\downarrow,\downarrow}$ , and (e)  $C_{g,l,l;m,m}^{\uparrow,\uparrow;\downarrow,\downarrow}$ . Here,  $l \neq m$ . (f) The first-order correction for  $\hat{\chi}_{\sigma,\sigma;\rho,\rho}^c(q)$ .

Next, we derive the matrix elements of the  $B_{1g}$  phonon mediated interaction. We show an example of schematic expression of  $B_{1g}$  phonon mode in Fig. S2(a). In Figs.

S2(b)-S2(e), we show the diagrammatic expression for the spin-dependent phonon-mediated interaction term:  $C_{g,l,l';m,m'}^{\sigma,\sigma';\rho,\rho}$ . Figure S2(f) shows the first-order correction by  $g$  for the spin-dependent susceptibilities  $\hat{\chi}^{\sigma,\sigma';\rho,\rho}(q)$  at  $\omega_j = 0$ . The first terms in Figs. S2(b)-S2(e) give the bubble diagrams, and the second term in Fig. S2(b) gives the ladder diagram. In the case of  $\omega_D \gg W_{\text{band}}$ , we can replace  $g(\epsilon_n - \epsilon_{n'})$  with the constant  $g$ , so both the bubble and ladder diagrams contribute to the susceptibility. Thus, the phonon-induced four-point vertex for  $\omega_D \gg W_{\text{band}}$  is

$$C_{g,l,l';m,m'}^s = \begin{cases} g & (l = l' = m = m') \\ -g & (l = m \neq l' = m') \\ 0 & (\text{otherwise}) \end{cases}, \quad (\text{S4})$$

$$C_{g,l,l';m,m'}^c = \begin{cases} +g & (l = l' = m = m') \\ -2g & (l = l' \neq m = m') \\ +g & (l = m \neq l' = m') \\ 0 & (\text{otherwise}) \end{cases}, \quad (\text{S5})$$

where  $\hat{C}_g^{c(s)} = \hat{C}_g^{\uparrow,\uparrow;\uparrow,\uparrow} + (-)\hat{C}_g^{\uparrow,\uparrow;\downarrow,\downarrow}$ . In the opposite case,  $\omega_D \ll W_{\text{band}}$ , the ladder diagrams are expected to be small. In fact, the corresponding irreducible susceptibility is approximately  $\chi_{l,l';m,m'}^{\text{ladder}}(q) \approx -\frac{T}{N_k} \sum_k G_{l,m}(k + q)G_{m',l'}(k)\theta(\omega_D - |\epsilon_n|)$ , which should be much smaller

than  $\chi_{l,l';m,m'}^0(q)$  due to  $\theta(\omega_D - |\epsilon_n|)$ . For this reason, the phonon-induced four-point vertex for  $\omega_D \ll W_{\text{band}}$  is

$$C_{g,l,l';m,m'}^s = 0, \quad (\text{S6})$$

$$C_{g,l,l';m,m'}^c = \begin{cases} +2g & (l = l' = m = m') \\ -2g & (l = l' \neq m = m') \\ 0 & (\text{otherwise}) \end{cases}. \quad (\text{S7})$$

Here,  $\hat{C}_g^c$  in Eq. (S7) corresponds to  $g_{l,l';m,m'}(\omega_j) \equiv -2g(\omega_j) \cdot \delta_{l,l'}\delta_{m,m'}(2\delta_{l,m} - 1)$  used in the main text. Since  $\hat{C}_g^s = 0$  in Eq. (S6),  $\alpha_S$  is independent of  $g$  for  $\omega_D \ll W_{\text{band}}$  in the RPA.

In the SC-VC theory, the charge-channel  $\chi$ -VC at  $q = 0$  is approximately proportional to  $\sum_p \{3\chi^s(p)^2 + \chi^c(p)^2\}$ . We have verified that the contribution to  $\hat{\Lambda}^c$  from  $\chi^s(q)$  dominates over that from  $\chi^c(q)$  even for  $\alpha_S \sim \alpha_C$ . For this reason, we can safely put  $g = 0$  in calculating the  $\chi$ -VC in the case of  $\omega_D \ll W_{\text{band}}$ .

### C: Expression for $U$ -VC

We explain the AL-type  $U$ -VCs, which were also introduced in Ref. [2]. The charge- and spin-channel AL-terms in Fig. 1(d) in the main text are given as

$$\Lambda_{l,l';m,m'}^{\text{AL},c}(k,k') = \frac{T}{2N_k} \sum_p \sum_{a,b,c,d,e,f} G_{a,b}(k' - p)\Lambda_{m,m';c,d,e,f}^{0'}(k - k', p) \\ \times \{I_{l,a;c,d}^c(k - k' + p)I_{b,l';e,f}^c(-p) + 3I_{l,a;c,d}^s(k - k' + p)I_{b,l';e,f}^s(-p)\}, \quad (\text{S8})$$

$$\Lambda_{l,l';m,m'}^{\text{AL},s}(k,k') = \frac{T}{2N_k} \sum_p \sum_{a,b,c,d,e,f} G_{a,b}(k' - p)\Lambda_{m,m';c,d,e,f}^{0'}(k - k', p) \\ \times \{I_{l,a;c,d}^c(k - k' + p)I_{b,l';e,f}^s(-p) + I_{l,a;c,d}^s(k - k' + p)I_{b,l';e,f}^c(-p)\} \\ + \delta\Lambda_{l,l';m,m'}^{\text{AL},s}(k,k'), \quad (\text{S9})$$

where  $\hat{I}^x(q) = \hat{U}^{0;x} + \hat{U}^{0;x}\hat{\chi}^x(q)\hat{U}^{0;x}$  in this SM. The three-point vertex  $\hat{\Lambda}^0(q,p)$  is given as

$$\Lambda_{l,l';a,b,e,f}^0(q,p) = -\frac{T}{N_k} \sum_{k'} G_{l,a}(k' + q)G_{f,l'}(k')G_{b,e}(k' - p), \quad (\text{S10})$$

and  $\Lambda_{m,m';c,d,g,h}^{0'}(q,p) \equiv \Lambda_{c,h;m,g;d,m'}^0(q,p) + \Lambda_{g,d;m,c;h,m'}^0(q,-p-q)$ . The last term in Eq. (S9) is given as

$$\delta\Lambda_{l,l';m,m'}^{\text{AL},s}(k,k') = \frac{T}{N_k} \sum_p \sum_{a,b,c,d,e,f} G_{a,b}(k' - p)I_{l,a;c,d}^s(k - k' + p)I_{b,l';e,f}^s(-p)\Lambda_{m,m';c,d,e,f}^{0''}(k - k', p), \quad (\text{S11})$$

where  $\Lambda_{m,m';c,d,g,h}^{0''}(q,p) \equiv \Lambda_{c,h;m,g;d,m'}^0(q,p) - \Lambda_{g,d;m,c;h,m'}^0(q,-p-q)$ . We verified that the contribution from Eq. (S11) is very small.

In addition,  $\hat{X}^x(q)$  is written by using the  $\hat{\Lambda}^{\text{AL},x}(k,k')$  as follows

$$X_{l,l';m,m'}^{s(c)}(q) = -\frac{T}{N_k} \sum_{k,a,b} G_{b,l'}(k)G_{l,a}(k + q)\Lambda_{b,a;m',m}^{\text{AL},s(c)}(k,k + q) - \chi_{l,l';m,m'}^0(q). \quad (\text{S12})$$

Finally, we summarize the approximations applied to the numerical study in the main text. In calculating the susceptibilities based on the SC-VC method, (i) we neglect the  $\chi$ -VC for spin channel  $\hat{X}^s$ , which has been justified in the five-orbital model as we discussed in Refs. [1, 3] in detail. (ii) We also neglect the ladder diagrams due to the phonon-mediated interaction for the susceptibilities, which is justified for  $\omega_D \ll W_{\text{band}}$ . In calculating the gap equation in the main text, (iii) we neglect the retardation effect by putting  $g(\omega_j) = g$  in the pairing interaction, and (iv) we drop the  $U$ -VC at finite  $\omega_j$ . The approximations (iii) and (iv) lead to the underestimation of the plain  $s_{++}$  wave state, so the region of the full-gap  $s_{++}$  wave state in Fig. 3(a) in the main text is underestimated.

#### D: Local approximation of $U$ -VC in the gap equation

In the main text, we performed the numerical study of  $U$ -VC, by taking account of its momentum dependence seriously. Figure S3(a) shows the superconducting phase diagram in the  $\alpha_S$ - $\alpha_C$  space, which is equivalent to the  $\alpha_S$ - $g$  phase diagram in Fig. 3(a) in the main text. However, this calculation is very time consuming, and it is very convenient if the local approximation is applicable for the  $U$ -VC. To check the validity of the local approximation, we calculate the averaged  $U$ -VC over the FSs,  $\hat{\Lambda}_{\text{loc}}^x(\epsilon_n, \epsilon_{n'}) = \langle \hat{\Lambda}^x(k, k') \rangle_{\mathbf{k}, \mathbf{k}' \in \text{FS}}$ , and analyze the gap equation by using this local  $U$ -VC.

Figure S3(b) shows the obtained superconducting phase diagram by using the  $\hat{\Lambda}_{\text{loc}}^x(\epsilon_n, \epsilon_{n'})$ . We see that the full-gap  $s_{++}$  state disappears in this case, and this phase diagram is almost equivalent to that given by the Migdal approximation in Fig. 3(e) in the main text. Therefore, the momentum dependence of the  $U$ -VC has to be taken into account seriously in solving the gap equation.

#### E: Filling dependence of the phase diagram

In the main text, we show the superconducting phase diagram for the filling  $n_e = 2.30$ . Here, we show the filling dependence of the superconducting phase. Figures S4(a) and S4(b) show the phase diagram of both singlet and triplet states as functions of the chemical potential  $\mu$  and  $g$ . The self-energy is not included in the present study. Here,  $n_e = 2.30$  corresponds to  $\mu = 0.50$ . At each  $\mu$ , we set  $U$  to satisfy the relation  $\alpha_S = 0.94$ . The charge Stoner factor  $\alpha_C$  increases with  $g$ , and the maximum value is set to  $\alpha_C = 0.98$ .

In Fig. S4(a), we show the obtained phase diagram when  $U$ -VC is taken into account. We find that the present two-orbital model shows rich superconducting phase diagram, and the full-gap  $s_{++}$  wave state corresponds to the largest eigenvalue for a wide range of fill-

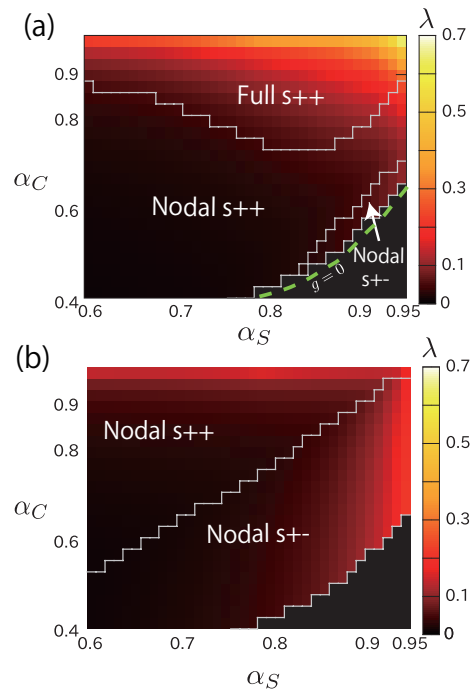


FIG. S3: (Color online) (a) The superconducting phase diagram in the  $\alpha_S$ - $\alpha_C$  space, which is equivalent to the  $\alpha_S$ - $g$  phase diagram in Fig. 3(a) in the main text. (b) Obtained phase diagram by using the  $U$ -VC in the local approximation.

ing parameter. It is noteworthy that the triplet superconductivity is appeared at  $\mu \approx 1.0$ , which corresponds to  $\text{Sr}_2\text{RuO}_4$ . This result is consistent with our previous study in Refs. [2, 4].

On the other hand, the  $s_{++}$  state disappears when we neglect the  $U$ -VC as shown in Fig. S4(b). Thus, we conclude that the  $U$ -VC plays an important role in realizing the full-gap  $s_{++}$  wave state for a wide parameter range.

#### F: Retardation effect

In the main text, we studied the spin and orbital fluctuations in the two-orbital Hubbard-Holstein model with the phonon-mediated interaction  $g(\omega_j) = g \frac{\omega_D}{\omega_D^2 + \omega_j^2}$ . In solving the gap equation, we neglect the retardation effect.

However, this simplification leads to the underestimation of the full-gap  $s_{++}$  wave state. Here, we study the case of  $\omega_D \ll T$ , that is,  $g(\omega_j) = g\delta_{j,0}$ . In this case, the retardation effect becomes maximum. The obtained phase diagram is given in Fig. S5. We find that the region of the full-gap  $s_{++}$  state is drastically expanded by the retardation effect.

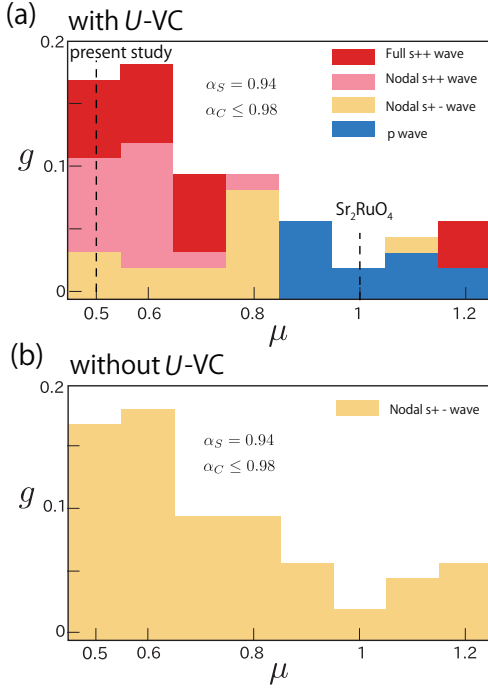


FIG. S4: (Color online) Phase diagram of the singlet and triplet states (a) with  $U$ -VC and (b) without  $U$ -VC as functions of  $\mu$  and  $g$ . At each  $\mu$ , we set  $U$  to satisfy the relation  $\alpha_S = 0.94$ . The electron filling for  $\text{Sr}_2\text{RuO}_4$  ( $n_e = 2.67$  for FS  $\alpha, \beta$ ) corresponds to  $\mu = 1.0$ . White color area corresponds to  $\alpha_C > 0.98$ . The orbital order is realized for  $\alpha_C > 1$ .

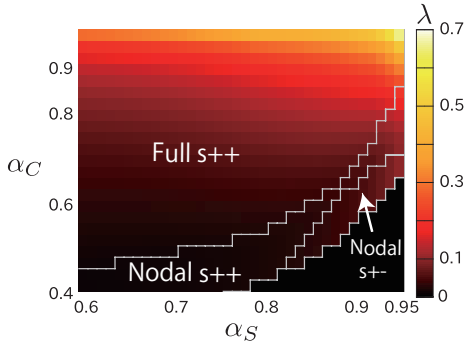


FIG. S5: (Color online) The phase diagram obtained by taking account of the retardation effect. The region of the full-gap  $s_{++}$  state is expanded by the retardation effect.

### G: Impurity effect on superconductivity

In the main text, we analyzed the superconducting gap equation based on the two-orbital Hubbard-Holstein model, in the absence of the impurity effect. However, it is well known that superconducting state is sensitively affected by impurities. Here, we analyze the gap equation in the presence of dilute non-magnetic impurities, using the  $T$ -matrix approximation. The gap equation in

the band basis is given as

$$\lambda \Delta^a(\mathbf{k}, \epsilon_n) = -\frac{T}{N_k} \sum_{a', \epsilon_m, \mathbf{k}'} |G_{a'}(\mathbf{k}', \epsilon_m)|^2 \Delta^{a'}(\mathbf{k}', \epsilon_m) \times \left[ V_{s(t)}^{a, a'}(\mathbf{k}, \epsilon_n, \mathbf{k}', \epsilon_m) - \frac{n_{\text{imp}}}{T} |T_{a, a'}(\mathbf{k}, \mathbf{k}', \epsilon_m)|^2 \delta_{n, m} \right], \quad (\text{S13})$$

which is schematically shown in Fig. S6(a).  $V_{s(t)}$  represents the singlet (triplet) pairing channel, which is given as  $\hat{V}_s = 3\hat{I}^{\Lambda, s}/2 - \hat{I}^{\Lambda, c}/2$ , and  $\hat{V}_t = -\hat{I}^{\Lambda, s}/2 - \hat{I}^{\Lambda, c}/2$ . Here,  $n_{\text{imp}}$  is the impurity concentration, and  $T_{a, a'}(\mathbf{k}, \mathbf{k}', \epsilon_m)$  is the impurity  $T$ -matrix with unitary scattering shown in Fig. S6(b). The Green function  $G_a(\mathbf{k}, \epsilon_n)$ , expressed as a double line in Fig. S6(a), contains the impurity-induced normal self-energy on band  $a$ ,  $\Sigma_a(k) = n_{\text{imp}} T_{a, a}(\mathbf{k}, \mathbf{k}, \epsilon_n)$ , shown in Fig. S6(c).

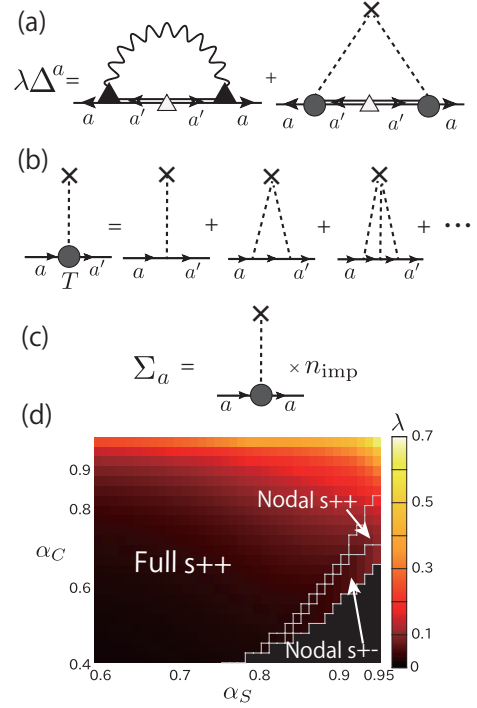


FIG. S6: (Color online) (a) Gap equation in the presence of impurities. (b)  $T$ -matrix given by the single impurity potential. (c) Impurity-induced self-energy. (d) The superconducting phase diagram for  $n_{\text{imp}} = 0.1\%$  in the  $\alpha_S$ - $\alpha_C$  space. The area of the full-gap  $s_{++}$  wave state is expanded by the impurity effect.

Figure S6(d) shows the superconducting phase diagram for  $n_{\text{imp}} = 0.1\%$  in the  $\alpha_S$ - $\alpha_C$  space. We find that the area of the full-gap  $s_{++}$  wave state is drastically expanded by the impurity effect even for  $n_{\text{imp}} = 0.1\%$ .

- [2] R. Tazai, Y. Yamakawa, T. Tsuchiizu, and H. Kontani, Phys. Rev. B **94**, 115155 (2016).
- [3] Y. Yamakawa, S. Onari, and H. Kontani, Phys. Rev. X **6**, 021032 (2016).
- [4] M. Tsuchiizu, Y. Yamakawa, S. Onari, Y. Ohno, and H. Kontani, Phys. Rev. B **91**, 155103 (2015).